ChemPubSoc Europe

DOI: 10.1002/chem.201400365

CHEMISTRY
A European Journal
Full Paper

Host–Guest Systems

Systematic Dissection of an Aminopyrrolic Cage Receptor for β-Glucopyranosides Reveals the Essentials for Effective Recognition

Oscar Francesconi,[b] Matteo Gentili,[b] Cristina Nativi,[b, c] Ana Ardá,[d] F. Javier Cañada,[d] Jesús Jiménez-Barbero,[d] and Stefano Roelens*[a]

Abstract: A set of structures designed for the recognition of glucosides has been obtained by systematically destructuring a tripodal aminopyrrolic cage receptor that selectively recognizes octyl-β-D-glucopyranoside (OctβGlc). NMR spectroscopy and isothermal titration calorimetry binding measurements showed that cleavage of one pillar of the cage was beneficial to the binding properties of the receptor, as long as two residual amino groups of the cleaved pillar were present. Removal of these two residual amino groups produced a dramatic loss of affinity for OctβGlc of the resulting monocyclic analogue of the parent cage receptor. A significant improvement in the binding ability was achieved by replacing one pillar with two aminopyrrolic hydrogen-bonding arms, despite the loss of a preorganized structure. In contrast to the cage receptor, recognition of OctβGlc was observed, even in a competitive medium (30% DMF in chloroform). Structural studies in solution, carried out through NMR spectroscopy and molecular modeling calculations, led to the elucidation of the 3D binding modes of the side-armed monocyclic receptors; this highlighted the key role of the amino groups and demonstrated the occurrence of a rotaxane-like complex, which featured the octyl chain of the glucoside threaded through the macrocyclic ring.

Introduction

Molecular recognition of carbohydrates is a topic of growing interest due to the crucial role exerted by saccharides in biological systems.[1] Exposed on the glycocalix as protein and lipid glycoconjugates, carbohydrates are involved in cell-to-cell, cell-to-bacteria, and cell-to-virus adhesion processes, which are governed by selective recognition of specific saccharidic epitopes.[1d] An increasing number of studies highlighted the importance of carbohydrates in pathogen recognition, in modulation of the immune system, and in the control of homeostasis and inflammation;[2] this explains why a molecular-level understanding of these processes is the main goal of current research.[3] To this end, synthetic receptors for selective recognition of specific carbohydrates of biological interest through noncovalent interactions, mimicking natural lectins,[4] have been developed to elucidate structural and functional requirements for effective recognition.[5]

In this context, in the last few years, we have developed a family of synthetic receptors for carbohydrates (cyclic and acyclic) that successfully recognize mono- and disaccharides in polar organic media.[6] The architecture of these receptors, common to the whole family, was based on a hexasubstituted aromatic scaffold, implemented with side arms featuring hydrogen-bonding groups, of which the aminopyrrolic chelating arrangement was the most effective binding combination. The idea behind this structural design was to combine hydrogen-bonding interactions between saccharidic hydroxyl groups and complementary hydrogen-bonding groups on the receptor, with CH–π and van der Waals interactions between the aromatic moiety and the aliphatic backbone of the carbohydrate, to construct a biomimetic receptor capable of recognizing saccharidic ligands through noncovalent interactions. Although recognition in water has not yet been achieved, the binding properties measured in organic solvents for the receptors developed so far shed light on the requirements for effective recognition.

Within this family of structures, bicyclic cage receptor **1** showed remarkable recognition properties, in that it selectively distinguished a β-glucoside (OctβGlc) from glycopyranosides of the manno and galacto series, featuring 20 μM affinity and complete β/α selectivity in chloroform.[7a] An investigation into the structure and binding properties of **1** by NMR spectroscopy and isothermal titration calorimetry (ITC) techniques,

[a] Dr. S. Roelens
Istituto di Metodologie Chimiche (IMC)
Consiglio Nazionale delle Ricerche (CNR), Dipartimento di Chimica
Polo Scientifico e Tecnologico, 50019 Sesto Fiorentino, Firenze (Italy)
E-mail: stefano.roelens@unifi.it

[b] Dr. O. Francesconi, M. Gentili, Prof. C. Nativi
Dipartimento di Chimica, Università di Firenze
Polo Scientifico e Tecnologico, 50019 Sesto Fiorentino, Firenze (Italy)

[c] Prof. C. Nativi
Centro Risonanze Magnetiche (CERM)
Polo Scientifico e Tecnologico, 50019 Sesto Fiorentino, Firenze (Italy)

[d] Dr. A. Ardá, Prof. F. J. Cañada, Prof. J. Jiménez-Barbero
Chemical and Physical Biology
Centro de Investigaciones Biológicas, CSIC
Ramiro de Maeztu 9, 28040 Madrid (Spain)

Supporting information for this article is available on the WWW under http://dx.doi.org/10.1002/chem.201400365.

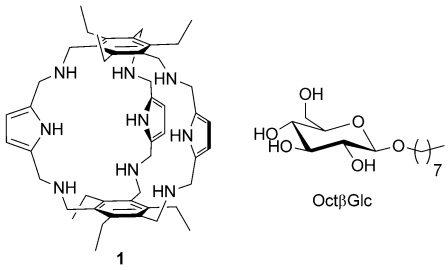

combined with molecular modeling calculations,[7b] revealed that the recognition ability of **1** resulted from the interplay of several factors, including the size of the bicyclic cage, the correct binding geometry, and the efficacy of the pyrrolic hydrogen-bonding groups, which cooperate for an energetically favorable binding of the all-equatorial glucoside inside the receptor cavity. Yet, when switching to more polar media, such as acetonitrile, receptor **1** unexpectedly failed to recognize the β-glucoside. This evidence led us to suspect that the shape-persistent cage might be somewhat too tight or too rigid to accommodate the saccharidic ligand when contending with a competitive solvent. This hypothesis was based on the observation that the CPK models of the complex showed the glucoside completely filling the cavity of the receptor, with little or no freedom of the guest to adjust to the cavity itself. Following this hypothesis, we thought that cleaving a bond in one of the pillars of the cage might relieve congestion and provide the appropriate adaptivity, while bringing minimal perturbation to the constitution of the receptor, providing that a cage-like geometry could be achieved by the resulting side-armed monocyclic structure upon binding. Further dissection of the cleaved pillar, destructuring the cage architecture down to the monocyclic core through a stepwise removal of all constituent elements of the side arm, would show the effectiveness of the bicyclic receptor with respect to the monocyclic counterpart and would shed light on the contribution to binding from the side chain. On the other hand, converting the monoarmed receptor into a double-armed chelating monocyclic receptor by implementing an additional binding arm would show whether recognition ability could be further improved.

Herein, we report the details of a study on the structure, dynamics, and binding properties of the receptors obtained by the aforementioned systematic modification of the parent receptor architecture. The investigation, carried out by NMR spectroscopy and ITC techniques, and by molecular modeling calculations, in addition to providing a 3D view of the recognition modes in solution, led to the quantification of 1) the large affinity difference for the glucoside between the constitutionally analogous mono- and bicyclic receptors; 2) the recognition improvement achieved by an adaptive structure, compared with the preorganized parent cage receptor; and 3) the substantial contribution to glucoside recognition from the hydrogen-bonding amino groups, both in terms of binding affinity and conformation-directing ability.

Results and Discussion

Design and synthesis

The systematic modifications designed for the structure of receptor **1** are outlined in Scheme 1. When cleaving one pillar of the cage, the least perturbing synthetically feasible modification consists of removing one of the two methylene groups adjacent to the pyrrolic moiety to give monocyclic structure **2**. Although devoid of the original bicyclic structure, the resulting receptor preserves all binding groups of the parent architecture. Subsequent removal of the pyrrole group from the side arm affords symmetric diamino compound **3**, which features a reduced number of hydrogen-bonding groups. Stepwise removal of the residual amino groups leads to compounds **4** and **5**, which, through loss of one entire pillar, containing three out of nine hydrogen-bonding groups of the parent structure, affords the monocyclic analogue of **1**. As an alternative to the described destructuring pathway, cleaved receptor **2** can be implemented with an additional pyrrole ring on the primary amino group, giving rise to the symmetrical, double-armed monocyclic structure **6**. In addition to the increased number of hydrogen-bonding groups, receptor **6** may endow the monocyclic structure with a chelating arrangement of

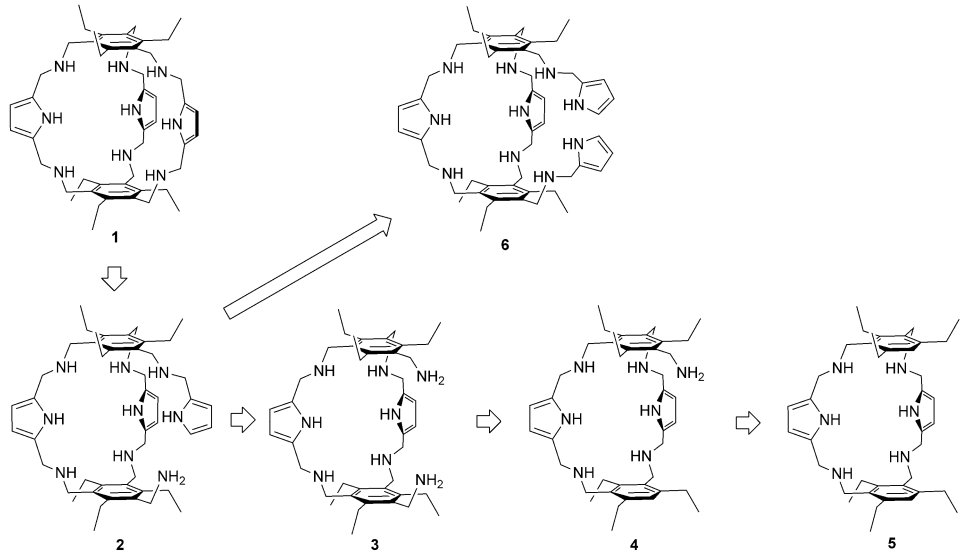

Scheme 1. Systematic modification of the structure of receptor **1**.

binding groups, which may improve affinity toward the glucosidic ligand.

Receptor **2** could be prepared through the convergent synthetic pathway described in Scheme 2. Compounds **7** and **8**, prepared from 1,3,5-tri(bromomethyl)-2,4,6-triethylbenzene, were treated with the sodium salt of trifluoroacetamide to give the corresponding trifluoroacetamides **9** and **10**, which underwent alkaline hydrolysis to afford the corresponding amines **11** and **12**. Monoamine **11** was condensed with pyrrole-2-carboxaldehyde to give the corresponding Schiff base, which was reduced to the aminopyrrolic compound **13**. On the other hand, diamine **12** was condensed with 5-(5,5-dimethyl-1,3-dioxan-2-yl)pyrrole-2-carbaldehyde, the monoprotected pyrrole dicarbaldehyde, and then reduced to compound **14**, which was deprotected to give dialdehyde **15**. Diamine **16**, which was obtained from **13** by Staudinger reduction, was condensed with **15** and the resulting cyclic Schiff base was reduced by sodium borohydride to give compound **17**. Staudinger reduction of **17** finally afforded receptor **2**.

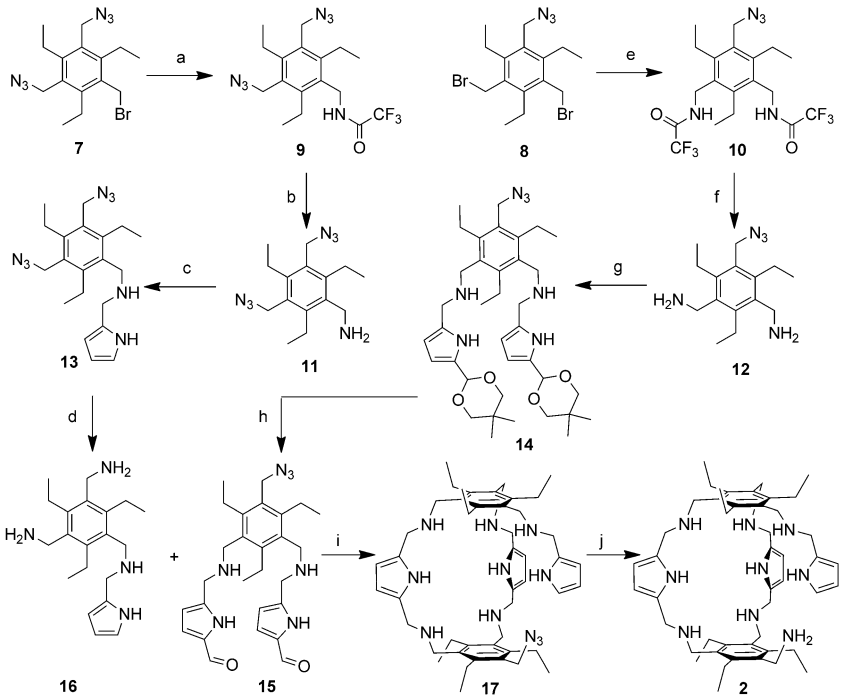

Scheme 2. Synthesis of receptor **2**. Reagents and conditions: a) trifluoroacetamide, NaH, DMF, RT, overnight, 88%; b) NaOH, CH_3OH/H_2O, RT, overnight, 98%; c) pyrrole-2-carbaldehyde, AcOH, $CHCl_3$, RT, overnight, then $NaBH_4$, CH_3OH, RT, 1 h, 84%; d) PPh_3, H_2O/THF, RT, overnight, 97%; e) trifluoroacetamide, NaH, DMF, RT, overnight, 84%; f) NaOH, CH_3OH/H_2O, RT, overnight, 97%; g) 5-(5,5-dimethyl-1,3-dioxan-2-yl)-1*H*-pyrrole-2-carbaldehyde, $CHCl_3$, RT, overnight, then $NaBH_4$, CH_3OH, RT, 1 h, 79%; h) HCl, H_2O/THF, RT, 2 h, $>$99%; i) $CHCl_3$, RT, overnight, then $NaBH_4$, CH_3OH, RT, 1 h, 96%; j) PPh_3, H_2O/THF, RT, overnight, 84%.

Receptors **3** and **4** were prepared from **12** and **15**, respectively, through the synthetic sequence outlined in Scheme 3, by condensation with the appropriate reagent, reduction of the imines to azides **18** and **19**, and subsequent Staudinger reduction. Receptor **5** was prepared by condensation of 1,3-bis(aminomethyl)-2,4,6-triethylbenzene with pyrrole-2,5-dicarboxaldehyde and subsequent reduction of the resulting cyclic Schiff base with sodium borohydride (Scheme 4).

Finally, receptor **6** was conveniently synthesized by condensing receptor **3** with pyrrole-2-carboxaldeyde (2 equiv), followed by reduction with sodium borohydride (Scheme 4).

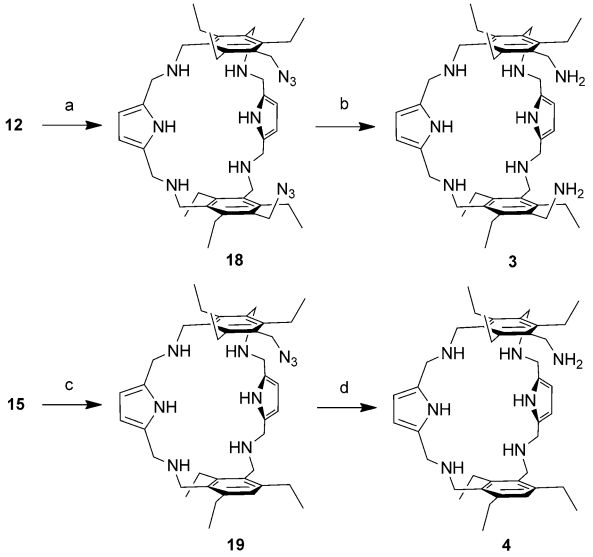

Scheme 3. Synthesis of receptors **3** and **4**. Reagents and conditions: a) pyrrole-2,5-dicarbaldehyde, $CHCl_3$, RT, overnight, then $NaBH_4$, CH_3OH, RT, 1 h, 87%; b) PPh_3, H_2O/THF, RT, overnight, 84%; c) 1,3-bis(aminomethyl)-2,4,6-triethylbenzene, AcOH, $CHCl_3$, RT, overnight, then $NaBH_4$, CH_3OH, RT, 1 h, 49%; d) PPh_3, H_2O/THF, RT, overnight, 93%.

Binding studies

To homogeneously compare the binding properties of the new set of monocyclic receptors with those of the parent cage receptor **1**, the binding affinities toward OctβGlc were assessed through ^{1}H NMR spectroscopic titrations in $CDCl_3$ at 298 K. Association constants were measured according to a previously described protocol,[6k] which consisted of the simultaneous fit of the complexation-induced shifts of all available signals from both the receptor and the glycoside to the appropriate association model by nonlinear regression analysis.

Analogously to receptor **1**, upon addition of receptors **2**, **3**, and **6**, the ^{1}H NMR spectra of OctβGlc showed the appearance of a new set of separated signals from those of the free glucoside; this revealed the formation of a 1:1 species under a slow-

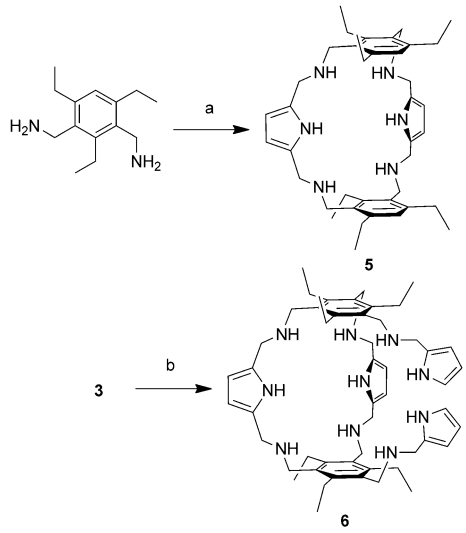

Scheme 4. Synthesis of receptors **5** and **6**. Reagents and conditions: a) pyrrole-2,5-dicarbaldehyde, $CHCl_3$, RT, overnight, then $NaBH_4$, CH_3OH, RT, 1 h, 57%; b) pyrrole-2-carbaldehyde, $CHCl_3$, RT, overnight, then $NaBH_4$, CH_3OH, RT, 1 h, 91%.

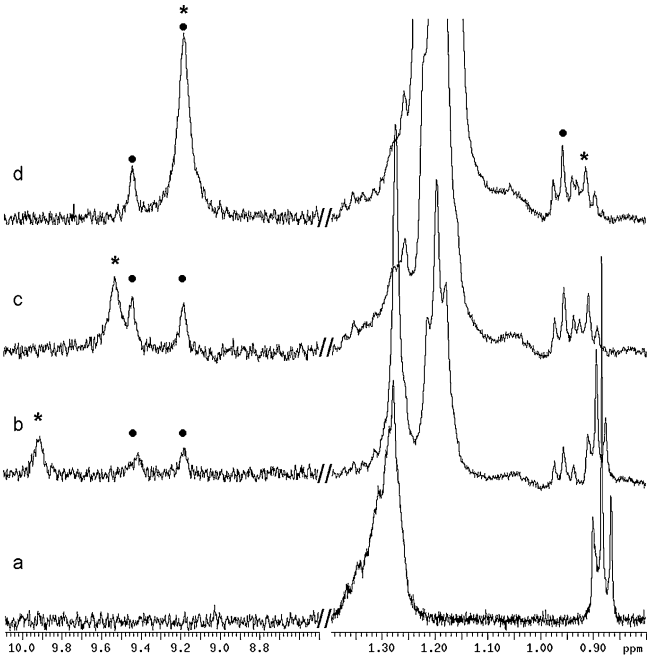

Figure 1. Selected spectral regions of the ^{1}H NMR spectroscopic titration (400 MHz, $CDCl_3$, 298 K) of OctβGlc (0.992 mM) with increasing concentrations of receptor **3**: a) 0, b) 0.429, c) 1.00, d) 2.00 mM. Left: pyrrolic NH signals; right: terminal octyl chain signals of OctβGlc. The signals of the Fast (*) and Slow (●) 1:1 complexes are also indicated.

exchange regime on the NMR spectroscopy timescale (Slow; Figure 1 and Figures S1 and S2 in the Supporting Information). However, although this was true for receptors **3** and **6**, receptor **2** revealed the presence of two different slow-exchanging 1:1 complexes, the signals of which increased along the titration. This behavior, which is clearly appreciated from the HSQC map (Figure S3 in the Supporting Information), can be explained by considering that the two halves of receptor **2**, with respect to the plane bisecting the pyrrole rings, are not symmetrical. Therefore, two distinct isomeric complexes are formed upon binding OctβGlc, namely, Slow(α) and Slow(β), which are caused by inclusion of the glucoside inside the receptor cleft with either the α or β face pointing toward the half of the receptor with the primary amine, respectively.

In addition to slow-exchanging complexes, all three receptors formed complex species in a fast-exchange regime on the NMR spectroscopy timescale that were not detected for cage receptor **1**. The fast-exchanging complexes (Fast) were revealed from the observed chemical shift variations of the OctβGlc signals along the titration with receptors **2**, **3**, and **6**. These chemical shift perturbations reflected the time-averaging of signals from the bound and unbound glucoside. Concomitantly, the receptor signals underwent significant variations of chemical shift as well, which further supported the formation of Fast complexes in solution. Although this evidence did not question the formation of the Slow complexes, it unavoidably affected the equilibrium concentration of free glucoside required for a quantitative calculation of binding constants, which, therefore, could not be assessed by NMR spectroscopic titrations. In contrast, receptors **4** and **5** featured the exclusive formation of the Fast complexes, which allowed the determination of the cumulative binding constants reported in Table 1. Because multiple complex species of different stoichiometries were found in some cases, affinities were assessed on a common scale from the measured binding constants through the BC_{50}^0 parameter, which is a binding descriptor that quantitatively defines the overall affinity of a receptor for a ligand.[8] The BC_{50}^0 (intrinsic median binding concentration) descriptor is defined as the total concentration of receptor necessary to bind 50%

Table 1. Cumulative formation constants ($\log\beta_n$) and intrinsic median binding concentrations (BC_{50}^0, [μM])[a] for receptor to glycoside (R/G) complexes of OctβGlc in $CDCl_3$.

Receptor	NMR[b]		ITC[c]	
	$\log\beta$ (R/G)	BC_{50}^0	$\log\beta$ (R/G)	BC_{50}^0
1	4.684 ± 0.008 (1:1)	20.7 ± 0.4	4.60 ± 0.01 (1:1) 7.57 ± 0.04 (1:2)	25.1 ± 0.6
2	n.a.[d]	n.a.[d]	5.09 ± 0.05 (1:1)	8.1 ± 0.9
3	n.a.[d]	n.a.[d]	5.02 ± 0.03 (1:1) 8.4 ± 0.1 (1:2)	9.2 ± 0.7
4	4.36 ± 0.07 (1:1) 6.9 ± 0.3 (2:1)	42.5 ± 6.6	4.41 ± 0.02 (1:1)	38.9 ± 2.0
5	3.11 ± 0.03 (1:1) 5.23 ± 0.05 (1:2)	674 ± 32	3.08 ± 0.01 (1:1)	831 ± 27
6	n.a.[d]	n.a.[d]	5.46 ± 0.05 (1:1)	3.5 ± 0.4

[a] Calculated from the $\log\beta$ values by using the "BC_{50} Calculator" program.[9] [b] Measured by ^{1}H NMR spectroscopy (400 MHz) from titration experiments at $T = 298$ K. [c] Measured by ITC from titration experiments at $T = 298$ K. [d] Not available: simultaneous presence of fast- and slow-exchanging complexes on the NMR spectroscopy timescale prevents calculation of the formation constants from NMR spectroscopy data.

of the ligand when the fraction of bound receptor is zero, that is, when forming the first complex molecule. This value coincides with the dissociation constant, K_d, for 1:1 complexes, whereas it can be viewed as a "global" dissociation constant when more than one complex is present in solution. The BC_{50}^0 values calculated for the investigated systems through the BC_{50} Calculator[9] are also reported in Table 1 and compared with values previously obtained for receptor **1**.

To correctly assess the affinities of receptors **2**, **3**, and **6**, and to confirm those obtained for receptors **4** and **5**, calorimetric ITC titrations were also performed under the same conditions ($CHCl_3$, 298 K). When necessary, the presence of multiple complex species was addressed by combining independent titrations run at different reactant concentrations into a simultaneous fit of all data to remove ambiguities in the definition of the model. The results are reported in Table 1, in Figure 2 and in Figures S4 and S5 in the Supporting Information, together with previous data for receptor **1**, as cumulative binding constants and BC_{50}^0 values. The overall 1:1 complex macrospecies, irrespective of the exchanging kinetics, were detected by the calorimetric technique; thus overcoming the issue of fast and slow exchange observed in the NMR spectroscopic titrations. The ITC results for receptors **4** and **5** were in good agreement with those observed by NMR spectroscopy, whereby the slight differences between the BC_{50}^0 values were ascribed to the low sensitivity of the ITC technique to higher stoichiometry species.

From the results reported in Table 1, it can be noted that cleavage of one pillar of the cage in **2** gave a threefold increase in affinity, which confirmed the hypothesis that converting the cage into an adaptive structure was beneficial to the receptor binding properties. Analysis of the thermodynamic parameters (Table S1 in the Supporting Information) showed that the affinity increase was enthalpic in origin, which compensated for the entropic loss caused by the larger loss of degrees of freedom experienced by the flexible receptor, with respect to the preorganized structure, upon binding. The marked enthalpic gain can be understood in terms of improved adaptivity of the armed monocyclic structure, which allows for an improved hydrogen-bonding match between the receptor and saccharidic ligand.

Interestingly, removal of the pyrrolic hydrogen-bonding group from the side arm in receptor **3** does not affect the affinity with respect to **2**. This unexpected result, apparently in contrast to the well-established contribution of the pyrrolic groups to binding,[6c,e,h,j,7b] may be due to either marginal participation of this pyrrole in binding for conformational reasons or because its contribution is counterbalanced by an overall weakening of the interaction, which is likely to be caused by the geometry imposed by the binding arm. This latter explanation is supported by molecular modeling studies (see below). Remarkably, monocyclic diamino receptor **3** exhibits an improved affinity with respect to the bicyclic cage receptor **1**, demonstrating that effective recognition is not necessarily ascribed to the cage structure.

The substantial contribution from the amine binding groups clearly emerged from the results obtained with receptors **4** and **5**, which showed a dramatic drop of affinity toward OctβGlc with respect to **3**. Removal of one of the two amine groups caused a fourfold affinity decrease, whereas a two orders of magnitude drop was observed for the bare monocyclic receptor when removing both amino groups from the structure. Furthermore, Slow complexes were absent for both receptors, which displayed Fast complexes exclusively; this indicated that the diamino compound enforced a binding geometry with common structural/kinetic features to those of the parent cage structure.

Finally, the active contribution from the pyrrolic binding arms was demonstrated by bibracchial receptor **6**, the affinity

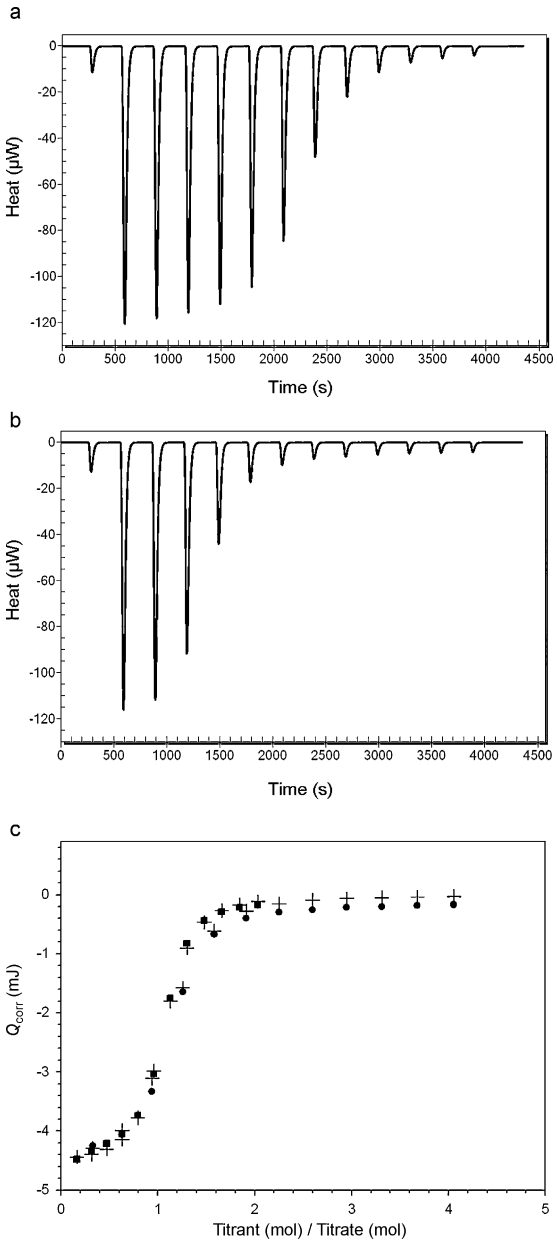

Figure 2. ITC titrations of OctβGlc with **2** in $CHCl_3$ at $T = 298$ K. a) Titration of OctβGlc (0.407 mM) with **2** (2.80 mM). b) Titration of OctβGlc (0.204 mM) with **2** (2.80 mM). c) Plot of the experimental and calculated data points obtained for titrations a) (■) and b) (●). Crosshair symbols (+) are calculated points obtained by simultaneous fit of all data through nonlinear regression.

of which for OctβGlc was the highest of the whole set of structures: three times larger than that of **2** and **3**, and eight times larger than that of **1**. As expected, pyrrolic groups contribute substantially to the binding ability of the receptor, whenever binding arms are not affected by conformational restrictions.

The results obtained for the monocyclic receptors show that the cage structure is not a prerequisite for effective recognition. Superior recognition properties could be achieved by a related monocyclic structure, when side arms with effective hydrogen-bonding groups were implemented in the architecture, providing that the appropriate binding geometry could be achieved, despite the unavoidable entropic loss upon complexation with respect to the preorganized bicyclic structure.

Encouraged by the excellent affinities obtained in chloroform, we challenged the recognition abilities of the investigated receptors in a more competitive medium to check whether evidence of binding could be detected where the cage receptor failed. The medium of choice was 30% DMF in chloroform, which provided good solubility of the reactants and hydrogen-bonding competitiveness comparable to that of acetonitrile.[6a] Cumulative binding constants toward OctβGlc, together with BC_{50}^0 values, measured by NMR spectroscopy in $CDCl_3$/DMF (70:30) for the set of receptors are presented in Table 2. Unexpectedly, receptors **2**, **3**, and **6**, together with Fast complexes, still showed the presence of Slow complexes, although less abundant; this indicated that binding was still substantial, even in the competitive solvent. Although the concomitant presence of Fast and Slow complexes did not allow the determination of the binding constants by NMR spectroscopic titrations, it clearly appeared that, in contrast to receptor **1**, recognition was not depleted by the competitive medium.

Table 2. Cumulative formation constants ($\log\beta_n$) and intrinsic median binding concentration (BC_{50}^0, [mM])[a] for receptor to glycoside (R/G) complexes of OctβGlc in $CDCl_3$/DMF 70:30.

Receptor	NMR[b]		ITC[c]	
	$\log\beta$ (R/G)	BC_{50}^0	$\log\beta$ (R/G)	BC_{50}^0
2	n.a.[d]	n.a.[d]	2.797 ± 0.007 (1:1)	1.59 ± 0.03
3	n.a.[d]	n.a.[d]	2.698 ± 0.006 (1:1)	2.01 ± 0.03
4	4.371 ± 0.006 (1:1)	4.25 ± 0.06	2.425 ± 0.001 (1:1)	3.76 ± 0.01
5	0.9 ± 0.2 (1:1)	114 ± 41	n.d.[e]	n.d.[e]
6	n.a.[d]	n.a.[d]	3.008 ± 0.008 (1:1)	0.98 ± 0.02

[a] Calculated from the $\log\beta$ values by using the BC_{50} Calculator program.[9] [b] Measured by ^{1}H NMR spectroscopy (400 MHz) from titration experiments at $T = 298$ K. [c] Measured by ITC from titration experiments at $T = 298$ K. [d] Not available: simultaneous presence of fast- and slow-exchanging complexes on the NMR timescale prevents calculation of the formation constants from the NMR spectroscopy data. [e] Not detectable.

Binding affinities could instead be assessed by ITC titrations for all receptors, with the exception of **5**, the affinity of which was negligible in this medium. Predictably, binding constants were depressed by two to three orders of magnitude with respect to those in chloroform; nevertheless, millimolar affinities could still be measured, for all but **5**, which featured very shallow selectivity that followed the same order as that observed in chloroform. Thermodynamic parameters, reported in Table S2 in the Supporting Information, confirmed the enthalpic origin of binding, as measured in chloroform, together with a similar adverse entropic contribution. In contrast to the parent cage receptor, hydrogen-bonding interactions established by the adaptive, side-armed monocyclic structures could favorably compete with the solvent for the glucoside, even in a largely polar medium.

Structural studies

The intriguing occurrence of concomitant Fast and Slow complexes in the recognition of OctβGlc prompted us to investigate the structural features of the recognition modes of the monocyclic receptors. Unfortunately, crystals suitable for X-ray structure determination could not be obtained for any of the complexes under study. Solution studies are more informative than solid-state studies when exploring dynamic phenomena, because they provide a closer description of dynamic processes. Elucidation of the 3D binding modes in solution for the most relevant complexes, in particular, of receptors **2**, **3**, and **6**, could be obtained by combining NMR spectroscopy data with molecular modeling calculations, following a well-established protocol.[10]

Basic information about the conformational features of complexes was retrieved from the chemical shift differences (CSD) observed between bound and unbound reactants. Chemical shifts for bound glucoside were obtained by adding an amount of receptor necessary to fully complex OctβGlc, as calculated from the measured binding constants. The results for the Fast and Slow complexes of **2**, **3**, and **6** are reported in Table 3 and Tables S3 and S4 in the Supporting Information, respectively, and depicted in Figure 3 and Figures S6 and S7 in the Supporting Information, respectively. The determination of the chemical shifts of the bound species, which was prevented by severe overlapping of signals in the ^{1}H spectra, was accomplished through 2D HSQC experiments that provided unambiguous shift values for all resonances.

The remarkable upfield shift of the glucoside signals observed in all three cases for both the Fast and Slow complexes clearly showed that the sugar experienced a shielding effect from the aromatic rings of

Table 3. Chemical shifts (δ, [ppm]) and chemical shift differences (CSD, [ppm]) of the proton signals of OctβGlc, free and bound to **2** (OctβGlc 1.59 mM, **2** 3.18 mM), for the Slow(α), Slow(β), and Fast complexes in $CDCl_3$ at 298 K.

Nucleus	Free	Slow(α)		Slow(β)		Fast	
		Bound	CSD	Bound	CSD	Bound	CSD
H-1	4.309	2.305	2.004	2.305	2.004	3.141	1.168
H-2	3.353	0.518	2.835	0.418	2.935	0.756	2.597
H-3	3.609	2.287	1.322	2.349	1.260	2.127	1.482
H-4	3.592	2.612	0.980	2.537	1.055	2.534	1.058
H-5	3.405	1.966	1.439	2.075	1.330	2.061	1.344
H-6	3.925	3.788	0.137	3.856	0.069	3.309	0.616
H-6′	3.825	3.571	0.254	3.571	0.254	3.309	0.516

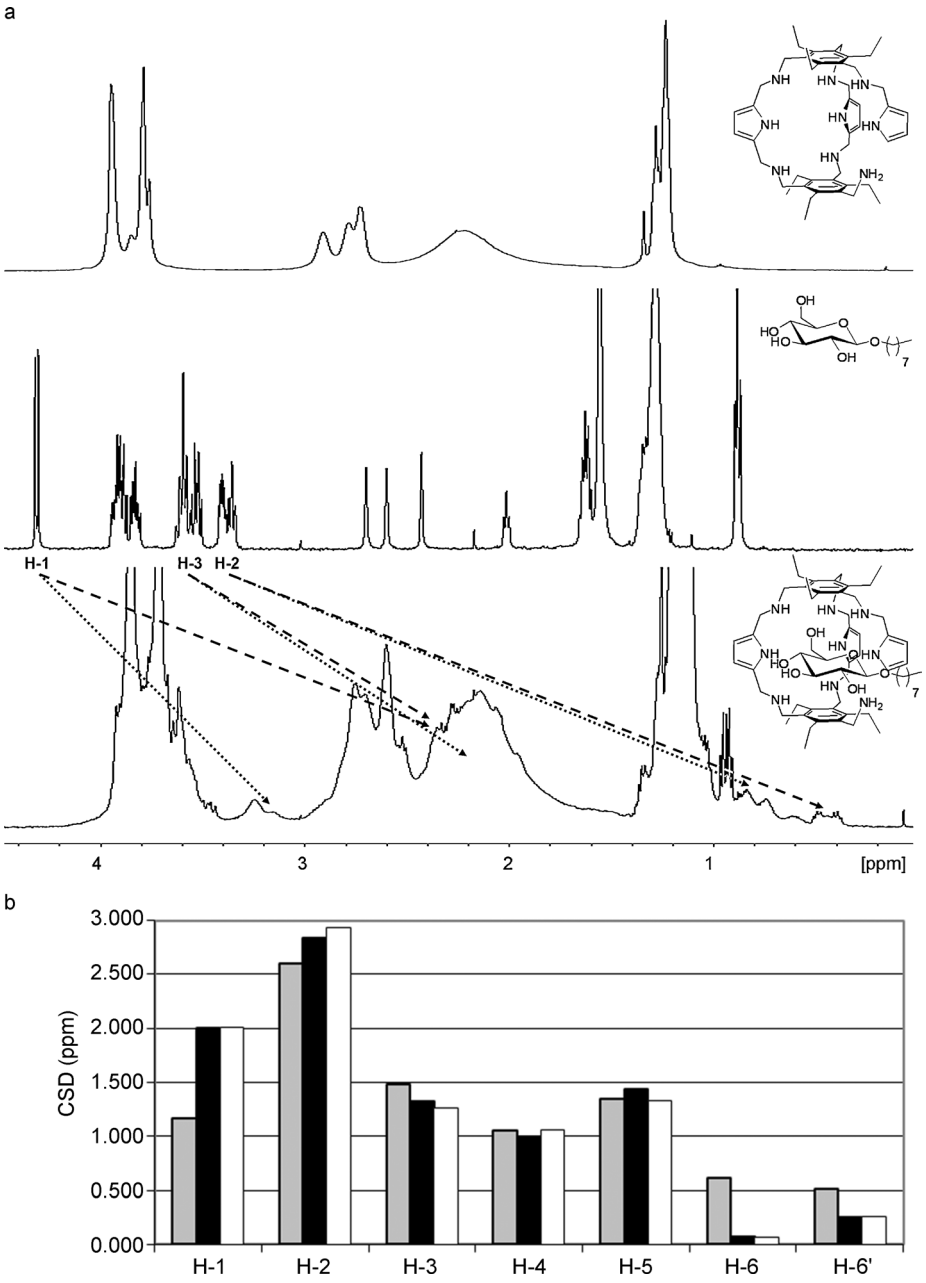

Figure 3. a) 500 MHz ^{1}H NMR spectra ($CDCl_3$, 298 K) of receptor **2** (top); OctβGlc (center); OctβGlc after the addition of two equivalents of receptor **2** (bottom). The arrows indicate chemical shift changes, as detected from 2D HSQC spectra (Figure S3 in the Supporting Information), of the ring protons of the sugar due to the formation of Fast (••••) and Slow (-----) complexes. b) Plot of the observed CSD between OctβGlc, free and in the presence of **2** (OctβGlc 1.59 mM, **2** 3.18 mM), for the Slow(α) (black), Slow(β) (white) and Fast (gray) complexes in $CDCl_3$ at 298 K.

the receptor. Furthermore, because the shielding affects hydrogen atoms on both sides of the sugar ring, it can be concluded that the receptor is bent into a cleft conformation and that OctβGlc lies inside the cleft between the two aromatic rings. The largest upfield shift displayed by the glucose H-1 and H-2 signals reveals that this portion of glucose is deeply located inside the cleft, more closely facing the aromatic rings. The similar CSD exhibited by the Fast and Slow complexes suggest that they may share similar binding modes, although displaying different dynamics, and that the slow kinetics, in analogy to those observed for the bicyclic structure **1**, may be due to hindrance from the cyclic part of the structure, causing slow motion of the complexation process.

Complementary information on the structures of the studied complexes was obtained by NOESY and ROESY experiments performed on mixtures of OctβGlc and receptors **2**, **3**, and **6**, from which several intermolecular NOE/ROE contacts were detected. A reasonable number of contacts could be identified for each of the three systems, the most significant of which have been reported in Table S5 in the Supporting Information and graphically depicted in Figure 4 for receptor **2**, and in Figures S8 and S9 in the Supporting Information for receptors **3** and **6**, respectively.

The observed NOE/ROE contacts for all Slow complexes exhibit close similarities, which suggest a common binding geometry. For example, the H-5 proton of glucose shows a ROE contact with the H-2 proton of the ethyl groups of the receptor; moreover, both the NH protons of the endocyclic pyrroles show intermolecular contacts with either the anomeric proton or the H-7 protons of the octyl chain. These proximities impose an orientation of the sugar in which the octyl chain threads the receptor macrocycle. Such a rotaxane-like geometry is also supported by the ROE contacts between the H-8 protons of the sugar and the H-24/30 protons of the ethyl groups residing within the macrocyclic environment of **2** and **3**, and with the H-13* methylene proton of **6**. This conformation may explain the slow kinetics observed for the Slow complexes, which may be caused by the sugar octyl chain threading the macrocycle to achieve the binding geometry. It should be noted that, in the case of receptor **2**, the occurrence of the two isomeric Slow(α) and Slow(β) complexes is demonstrated by the fact that the sugar H-8 proton simultaneously shows two different ROE contacts with the ethyl proton

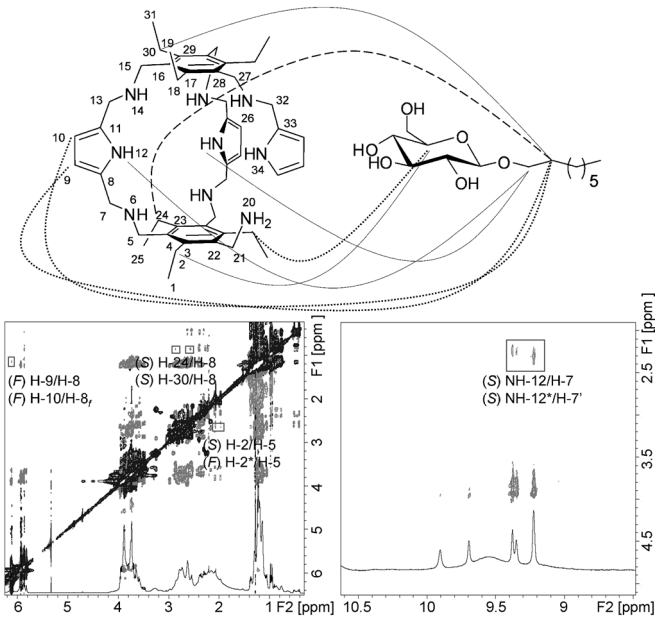

Figure 4. Top: Schematic representation of the intermolecular ROEs found between **2** and OctβGlc. ROE contacts unambiguously assigned to Slow(β) and Fast complexes are indicated by dashed and dotted lines, respectively. Bottom: 600 MHz ROESY spectrum of a 1:2 mixture of OctβGlc and **2** in CDCl3 at 298 K. Intermolecular ROE cross-peaks assigned to Fast (*F*) and Slow (*S*) complexes are indicated by squares.

H-30 and with the opposite ethyl proton H-24; this confirms the two different orientations of the sugar.

Concerning the Fast complexes, because of severe overlap of the signals, only a few of the several ROE cross-peaks could be unambiguously assigned to intermolecular contacts. Nevertheless, in the case of receptor **2**, the contact between the H-5 proton of the sugar and the H-2* proton of the ethyl group of the receptor remote from the macrocycle, together with the two contacts of the H-8 proton of the octyl chain with the pyrrolic H-9 and H-10 protons, impose a binding geometry in which the octyl chain of the sugar resides outside the receptor macrocycle; this is in agreement with the fast kinetics observed. Analogous contacts involving the octyl chain of the sugar were found in the complexes of **3** and **6**, which confirmed a binding geometry similar to that of **2**.

Because CSD and NOE/ROE contacts cannot fully define the binding geometries of the investigated complexes, a well-tested molecular mechanics computational protocol was applied to model the three-dimensional binding modes of OctβGlc with **2**, **3**, and **6**. The protocol consists of exploring the conformational space of the complex to find the families of structures in agreement with the experimental NMR spectroscopy data. In the first step, a conformational search was run on the free receptors in the absence of the glucoside. The result of the calculation was a pool of conformations that showed no significant energy minima. This behavior indicated that the monocyclic architecture was endowed with high flexibility, as opposed to the parent receptor **1**, which exhibited a shape-persistent preorganized cavity. In contrast, when the conformational search was run on the OctβGlc complex, the calculation returned three different families of structures for receptor **2**, each family was selected to include the structures found within an energy window of 10 kJ mol^{-1} from the minimum (Figure S10 in the Supporting Information), and two different families for receptors **3** and **6** (Figures S11 and S12 in the Supporting Information), which were in agreement with the NMR spectroscopy data; all structures found showed a well-defined cleft conformation for the receptor enclosing the bound glucoside. The results from calculations indicate that glucoside recognition drives the flexible, unbiased structure of the receptor to achieve a cleft conformation upon binding.

In Figures 5, 6 and 7, the minimum energy structures of the families obtained for the complexes of receptors **2**, **3**, and **6** are depicted, respectively, showing two different types of geometries: a) a "threaded" geometry, featuring the octyl chain threaded through the macrocycle; and b) an "unthreaded" geometry, featuring the octyl chain located outside the macrocycle. Both geometries feature the glucose moiety nested inside the receptor cleft, roughly orthogonal to each other, and parallel to the aromatic rings. Notably, both geometries allow the formation of several hydrogen-bonding interactions, which involve not only the pyrrolic rings, but also the aminic groups.

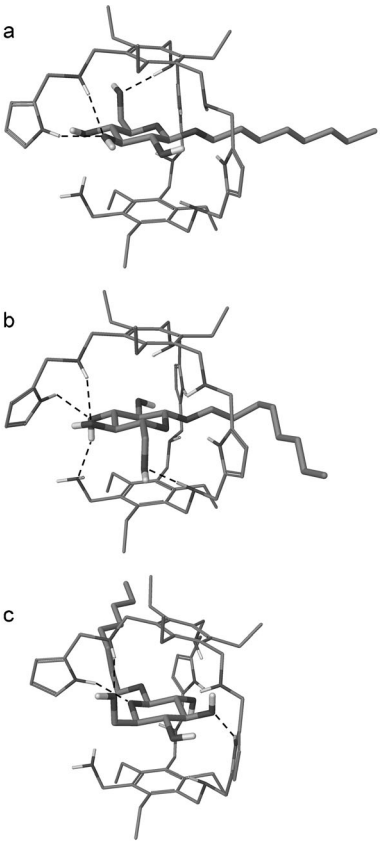

Figure 5. Minimum energy structures of the three families of complexes between **2** and OctβGlc obtained from the conformational search and compatible with the NMR spectroscopy data. Hydrogen bonds between the receptor and carbohydrate are depicted as dashed lines. Selected hydrogen-bond lengths: a) N–H···OH-3, 2.09 Å; N–H···OH-3, 2.10 Å; N–H···OH-6, 2.00 Å.; b) N–H···OH-3, 2.25 Å; O–H-3···NH, 2.17 Å; N–H···OH-4, 2.19 Å; N–H···OH-6, 2.01 Å. c) N–H···OH-3, 1.99 Å; N–H···O-5, 2.06 Å; N–H···OH-6, 2.06 Å.

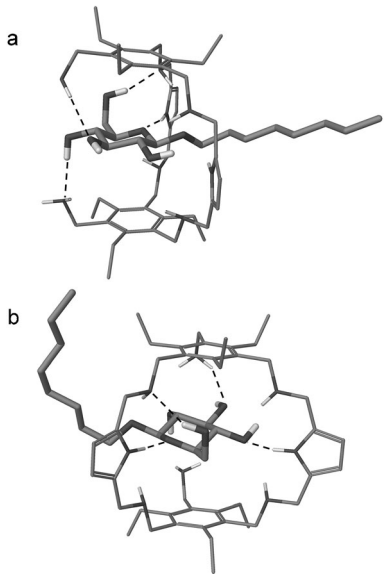

Figure 6. Minimum energy structures of the two families of complexes between **3** and OctβGlc obtained from the conformational search and compatible with the NMR spectroscopy data. Hydrogen bonds between the receptor and carbohydrate are depicted as dashed lines. Selected hydrogen-bond lengths: a) N–H···OH-3, 2.12 Å; O–H-4···NH, 2.09 Å; N–H···O-5, 2.04 Å; O–H-6···NH, 2.12 Å; b) N–H···OH-3, 2.11 Å; N–H···OH-4, 2.04 Å; N–H···O-5, 2.00 Å; O–H-6···NH, 2.18 Å.

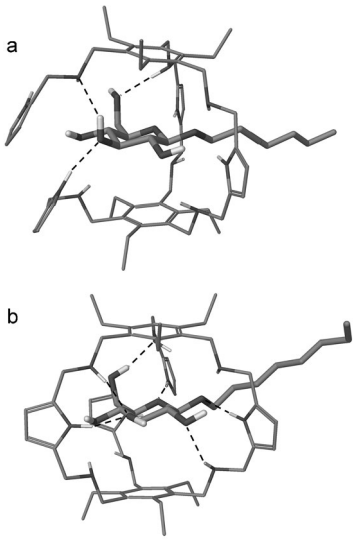

Figure 7. Minimum energy structures of the two families of complexes between **6** and OctβGlc obtained from the conformational search and compatible with the NMR spectroscopy data. Hydrogen bonds between the receptor and carbohydrate are depicted as dashed lines. Selected hydrogen-bond lengths: a) N–H···OH-3, 2.12 Å; O–H-3···NH, 2.15 Å; N–H···OH-6, 2.04 Å; b) N–H···OH-1, 2.03 Å; N–H···OH-2, 2.26 Å; N–H···OH-3, 1.94 Å; N–H···OH-3, 2.02 Å; N–H···O-5, 2.03 Å; O–H-6···NH, 2.05 Å.

Even in the absence of pyrrolic rings, amine groups are responsible for bending the structure into the cleft conformation. Good agreement between the experimental NOE/ROE contacts and the corresponding distances obtained from the calculated structures can be appreciated from Table 4, in which interatomic distances for Slow and Fast complexes of receptors **2**, **3**, and **6** are reported.

Thus, the observed Slow and the Fast complexes, that is, adducts showing slow and fast kinetics, are associated with threaded and unthreaded geometries, respectively. This may account for the kinetic phenomenology by considering that threading necessarily requires a conformational reorganization of the octyl chain, which slows down the binding process, whereas no reorganization is required for binding in the unthreaded geometry. Furthermore, the difference between the two isomeric Slow(α) and Slow(β) complexes of **2** can be perceived from Figure 5a and b, which shows a closely related geometry for the two structures, with the exception of a 180° rotation of the glucose moiety with respect to the C1–C4 axis.

Unambiguous support for the above interpretation of threading as the cause of slow kinetics was obtained by replacing the octyl chain with a methyl group in the aglycon moiety. Titration of **3** with increasing amounts of methyl-β-glucoside (MeβGlc) in $CDCl_3$/DMF 70:30 showed the exclusive formation of Fast complexes, with one single set of signals shifting upon complexation and no evidence of Slow adducts (Figure S13 in the Supporting Information), even though the affinities measured were comparable to those obtained for OctβGlc (NMR spectroscopy: $BC_{50}^0 = (3.8 \pm 0.1)$ mM; ITC: $BC_{50}^0 = (3.69 \pm 0.03)$ mM; cf. Table 2). Clearly, without the octyl chain, the threaded conformation does not occur and fast kinetics are restored.

An inventory of the hydrogen-bonding interactions has been obtained by choosing, from the calculated minimum energy structures, all O···N interatomic distances shorter than

Table 4. Intermolecular most intense NOE/ROE cross-peaks found in NOESY and ROESY spectra for complexes of OctβGlc with **2**, **3**, and **6**, and corresponding distances [Å] obtained from the calculated minimum energy structures.[a]

OctβGlc·**2**			OctβGlc·**3**		OctβGlc·**6**	
Slow(α)	Slow(β)	Fast	Slow	Fast	Slow	Fast
H-5/H-2 (2.87)	H-7/NH-12 (2.57)	H-5/H-2* (2.89)	H-1/NH-12 (3.49)	H-8/H-13* (4.42)	H-1/NH-12* (3.05)	H-7′/H-7* (2.93)
H-7/NH-12 (2.10)	H-7′/NH-12* (2.04)	H-8/H-9 (3.31)	H-1/NH-12 (3.47)		H-2/H-18* (3.05)	H-8/H-18 (2.67)
H-7′/NH-12* (2.55)	H-8/H-24 (2.48)	H-8/H-10 (3.59)	H-5/H-2 (2.76)		H-4/NH-34 (3.74)	
H-8/H-30 (2.43)			H-8/H-30 (2.39)		H-5/H-2 (3.12)	
					H-7/NH-12 (2.17)	
					H-8′/H-13* (3.17)	

[a] Nuclei that became nonequivalent upon complexation are marked with an asterisk.

the sum of the van der Waals radii, and selecting those distances that comply with hydrogen-bonding criteria. The results of such an inventory are collected in Table 5, from which it is evident that the observed complex stabilities are determined by a significant number of hydrogen-bonding interactions. In particular, it can be appreciated that the contribution from the aminic groups to the hydrogen-bonding network is prevalent, involving 16 out of a total of 27 interactions. The most dramatic drop in affinity is observed for the stepwise loss of two amino groups in **4** and **5**. The anticipated conformational origin of the very similar affinities exhibited by **2** and **3** finds a rationale in the changes induced by the pyrrolic binding arm on the hydrogen-bonding network. Indeed, in both the Slow and Fast complexes, hydrogen bonds established by this pyrrole pulls glucose slightly out of the cleft, which causes the loss of a hydrogen-bonding interaction of the sugar with one of the endocyclic pyrroles. This feature compensates for the advantage of the new interaction and leaves the affinity unchanged with respect to **3**. In contrast, the introduction of a second pyrrolic binding arm into the architecture significantly increases the number of hydrogen-bonding interactions by pushing glucose closer to the macrocycle, with which it can establish an additional hydrogen bond. Because the added binding arm does not itself participate in hydrogen bonding, its contribution most likely consists of sealing the receptor's cavity through nonbonding interactions. Interestingly, whereas for **2** and **3** the contribution of the Slow and Fast complexes to the overall conformer population is comparable, counterintuitively, for **6**, the contribution of the Fast complex becomes prevalent, so that the increase in affinity for OctβGlc can be ascribed mainly to the unthreaded structure. This evidence can, however, be easily explained on the basis of the six hydrogen-bonding interactions, provided by three chelating aminopyrrolic units, established by the unthreaded structure, which is the largest number of interactions of the whole set.

Table 5. Hydrogen-bonding interactions and corresponding distances [Å][a] found in the calculated minimum energy structures of the threaded and unthreaded complexes of OctβGlc with receptors **2**, **3**, and **6**.[b]

OctβGlc	OctβGlc·**2**			OctβGlc·**3**		OctβGlc·**6**	
	threaded (α)	threaded (β)	unthreaded	threaded	unthreaded	threaded	unthreaded
O-1							NH-12 (3.07)
OH-2							NH-6 (3.05)
OH-3	NH-34 (2.91)	NH-34 (2.94)	NH-12* (2.86)	NH_2-26 (3.01)	NH_2-26 (2.98)	NH-37 (3.03)	NH-12* (2.83)
	NH-26 (3.05)	NH_2-20 (3.04)				NH-26 (3.01)	NH-14* (2.96)
OH-4		NH-26 (3.00)		NH_2-20 (3.04)	NH-12 (2.83)		
O-5			NH-34 (3.03)	NH-12 (3.03)	NH-12* (3.00)		NH-34 (3.03)
OH-6	NH-14 (3.07)	NH-6* (3.02)	NH-26 (3.05)	NH-14 (3.03)	NH-14* (3.07)	NH-14 (3.04)	NH-26 (2.98)

[a] Interatomic distances shorter than the sum of van der Waals radii and complying with hydrogen-bonding criteria. [b] Nuclei that became nonequivalent upon complexation are marked with an asterisk.

Conclusion

We have shown that converting a preorganized cage receptor into a closely related adaptive structure results in an architecture endowed with improved binding properties, despite the loss of the preorganization advantage. The improvement relies on the ability of the flexible structure to establish a larger number of, or stronger, hydrogen-bonding interactions by more closely matching the binding requirements of the glucosidic guest. A further advantage of the side-armed flexible architecture is the conveniently accessible modification of the core structure to optimize recognition properties.

The systematic dissection of the architecture of the parent cage receptor revealed the contribution from the aminopyrrolic binding arrangement to the recognition properties of the receptor, as well as to the conformational behavior of the structure upon binding. In particular, it has been shown that amino groups provide not only a substantial contribution to the overall affinity, but also the driving force for bending the monocyclic structure into a cleft conformation.

A rationale for the intriguing occurrence of concomitant slow and fast exchanging 1:1 complexes on the NMR spectroscopy timescale was provided by combining experimental NMR spectroscopy data and molecular modeling calculations, which, besides giving a description of the 3D binding modes in solution, revealed the existence of two distinct types of glucoside complexes—a rotaxane-like threaded adduct and an unthreaded structure—that account for the observed kinetics, while cooperatively contributing to the overall binding affinity.

The most interesting conclusion appears to be the finding that effective recognition in a polar competitive medium can indeed be achieved by carefully designed adaptive structures endowed with aminopyrrolic hydrogen-bonding arrangements. This finding is a step forward in the design of synthetic receptors for the recognition of carbohydrates in a physiological medium.

Acknowledgements

This work has been carried out in the frame of the COST Action CM1102. High-field NMR spectra were acquired at the Magnetic Resonance Center (CERM) facilities of the Università di Firenze. We thank M. Lucci for technical assistance. Dr. A. Minoja from Bruker Italia s.r.l. is gratefully acknowledged for kind assistance. Ente Cassa di Risparmio di Firenze (Italy) is acknowledged for granting an ITC nano calorimeter (grant no. 2009.0576).

Keywords: carbohydrates · hydrogen bonds · molecular recognition · receptors · structure elucidation

[1] a) H.-J. Gabius, S. André, J. Jiménez-Barbero, A. Romero, D. Solís, *Trends Biochem. Sci.* **2011**, *36*, 298 – 313; b) *The Sugar Code: Fundamentals of Glycosciences* (Ed.: H.-J. Gabius), Wiley-VCH, Weinheim, **2009**; c) H. E. Murrey, L. C. Hsieh-Wilson, *Chem. Rev.* **2008**, *108*, 1708 – 1731; d) T. K. Lindhorst, *Essentials of Carbohydrate Chemistry and Biochemistry*, Wiley-VCH, Weinheim, 3rd ed., **2007**; e) *Carbohydrates in Chemistry and Biology* (Eds.: B. Ernst, G. W. Hart, P. Sinaÿ), Wiley-VCH, Weinheim, **2000**, Part I, Vol. 2 and Part II, Vol. 4.

[2] a) Y. van Kooyk, G. A. Rabinovich, *Nat. Immunol.* **2008**, *9*, 593 – 601; b) C. N. Scanlan, J. Offer, N. Zitzmann, R. A. Dwek, *Nature* **2007**, *446*, 1038 – 1045; c) D. R. Burton, R. A. Dwek, *Science* **2006**, *313*, 627 – 628; d) N. L. Letvin, *Nat. Rev. Immunol.* **2006**, *6*, 930 – 939; e) D. H. Dube, C. R. Bertozzi, *Nat. Rev. Drug Discovery* **2005**, *4*, 477 – 487; f) R. Medzhitov, C. A. Janeway, Jr., *Science* **2002**, *296*, 298 – 300.

[3] a) J. Arnaud, A. Audfray, A. Imberty, *Chem. Soc. Rev.* **2013**, *42*, 4798 – 4813; b) J. Balzarini, *Nat. Rev. Microbiol.* **2007**, *5*, 583 – 597; c) A. Imberty, E. P. Mitchell, M. Wimmerová, *Curr. Opin. Struc. Biol.* **2005**, *15*, 525 – 534; d) M. R. Pratt, C. R. Bertozzi, *Chem. Soc Rev.* **2005**, *34*, 58 – 68; e) C. R. Bertozzi, L. L. Kiessling, *Science* **2001**, *291*, 2357 – 2363.

[4] a) C. Ke, H. Destecroix, M. P. Crump, A. P. Davis, *Nat. Chem.* **2012**, *4*, 718 – 723; b) B. Sookcharoenpinyo, E. Klein, Y. Ferrand, D. B. Walker, P. R. Brotherhood, C. Ke, M. P. Crump, A. P. Davis, *Angew. Chem.* **2012**, *124*, 4664 – 4668; *Angew. Chem. Int. Ed.* **2012**, *51*, 4586 – 4590; c) N. P. Barwell, M. P. Crump, A. P. Davis, *Angew. Chem.* **2009**, *121*, 7809 – 7812; *Angew. Chem. Int. Ed.* **2009**, *48*, 7673 – 7676; d) Y. Ferrand, M. P. Crump, A. P. Davis, *Science* **2007**, *318*, 619 – 622.

[5] For recent reviews, see: a) A. P. Davis, *Nature* **2010**, *464*, 169 – 170; b) S. Jin, Y. Cheng, S. Reid, M. Li, B. Wang, *Med. Res. Rev.* **2010**, *30*, 171 – 257; c) D. B. Walker, G. Joshi, A. P. Davis, *Cell. Mol. Life Sci.* **2009**, *66*, 3177 – 3191; d) A. P. Davis, *Org. Biomol. Chem.* **2009**, *7*, 3629 – 3638; e) M. Mazik, *Chem. Soc. Rev.* **2009**, *38*, 935 – 956; f) S. Kubik, *Angew. Chem.* **2009**, *121*, 1750 – 1753; *Angew. Chem. Int. Ed.* **2009**, *48*, 1722 – 1725; g) A. P. Davis, T. D. James, in *Functional Synthetic Receptors* (Eds.: T. Schrader, A. D. Hamilton), Wiley-VCH, Weinheim, **2005**, pp. 45 – 109.

[6] a) O. Francesconi, C. Nativi, G. Gabrielli, M. Gentili, M. Palchetti, B. Bonora, S. Roelens, *Chem. Eur. J.* **2013**, *19*, 11742 – 11752; b) C. Nativi, O. Francesconi, G. Gabrielli, I. De Simone, B. Turchetti, T. Mello, L. Di Cesare Mannelli, C. Ghelardini, P. Buzzini, S. Roelens, *Chem. Eur. J.* **2012**, *18*, 5064 – 5072; c) C. Nativi, O. Francesconi, G. Gabrielli, A. Vacca, S. Roelens, *Chem. Eur. J.* **2011**, *17*, 4814 – 4820; d) A. Ardá, F. J. Cañada, C. Nativi, O. Francesconi, G. Gabrielli, A. Ienco, J. Jiménez-Barbero, S. Roelens, *Chem. Eur. J.* **2011**, *17*, 4821 – 4829; e) M. Cacciarini, C. Nativi, M. Norcini, S. Staderini, O. Francesconi, S. Roelens, *Org. Biomol. Chem.* **2011**, *9*, 1085 – 1091; f) A. Ardá, C. Venturi, C. Nativi, O. Francesconi, G. Gabrielli, F. J. Cañada, J. Jiménez-Barbero, S. Roelens, *Chem. Eur. J.* **2010**, *16*, 414 – 418; g) A. Ardá, C. Venturi, C. Nativi, O. Francesconi, F. J. Cañada, J. Jiménez-Barbero, S. Roelens, *Eur. J. Org. Chem.* **2010**, 64 – 71; h) C. Nativi, M. Cacciarini, O. Francesconi, G. Moneti, S. Roelens, *Org. Lett.* **2007**, *9*, 4685 – 4688; i) M. Cacciarini, E. Cordiano, C. Nativi, S. Roelens, *J. Org. Chem.* **2007**, *72*, 3933 – 3936; j) C. Nativi, M. Cacciarini, O. Francesconi, A. Vacca, G. Moneti, A. Ienco, S. Roelens, *J. Am. Chem. Soc.* **2007**, *129*, 4377 – 4385; k) A. Vacca, C. Nativi, M. Cacciarini, R. Pergoli, S. Roelens, *J. Am. Chem. Soc.* **2004**, *126*, 16456 – 16465.

[7] a) O. Francesconi, A. Ienco, G. Moneti, C. Nativi, S. Roelens, *Angew. Chem.* **2006**, *118*, 6845 – 6848; *Angew. Chem. Int. Ed.* **2006**, *45*, 6693 – 6696; b) O. Francesconi, M. Gentili, S. Roelens, *J. Org. Chem.* **2012**, *77*, 7548 – 7554.

[8] A. Vacca, O. Francesconi, S. Roelens, *Chem. Rec.* **2012**, *12*, 544 – 566.

[9] BC_{50} Calculator is a computer program developed for PC platforms and is available for free upon request from the corresponding author. A detailed description of the equations used by the program for computing BC_{50} and BC^{0}_{50} is reported in previous papers, see refs. [6c], [6j], and [8].

[10] For examples of the application of NMR spectroscopy techniques assisted by molecular modeling, see: a) J. Jiménez-Barbero, E. Dragoni, C. Venturi, F. Nannucci, A. Ardá, M. Fontanella, S. André, F. J. Cañada, H. J. Gabius, C. Nativi, *Chem. Eur. J.* **2009**, *15*, 10423 – 10431; b) M. Kolympadi, M. Fontanella, C. Venturi, S. André, H. J. Gabius, J. Jiménez-Barbero, P. Vogel, *Chem. Eur. J.* **2009**, *15*, 2861 – 2873; c) S. Mari, F. J. Cañada, J. Jiménez-Barbero, A. Bernardi, G. Marcou, I. Motto, I. Velter, F. Nicotra, B. La Ferla, *Eur. J. Org. Chem.* **2006**, 2925 – 2933; d) S. Mari, H. Posteri, G. Marcou, D. Potenza, F. Micheli, F. J. Cañada, J. Jiménez-Barbero, A. Bernardi, *Eur. J. Org. Chem.* **2004**, 5119 – 5225.

Received: January 28, 2014
Published online on April 3, 2014